

Fig. 6. Endothelium-independent vasodilation in coronary microvessels before and after I/R. The vasodilation is comparable under all conditions.

disturbed tight junctions between endothelial cells may be found by electronmicroscopical examination (21). With edaravone administration, NO bioavailability in the ischemic area endothelial layer of microvessels was significantly augmented (Fig. 3). In other settings, edaravone has also been shown to improve peripheral flow-mediated dilatation in smokers (22). Taken together, free radical scavenging by edaravone in the vessels results in preservation of NO availability and thereby maintains endothelial function, which is crucial for the cardiovascular system in both the short-term and long-term.

#### *Edaravone preserves nitric oxide and eNOS*

We have previously shown that endothelium-dependent vasodilation by acetylcholine would increase NO release in coronary circulation, indicating the central role of NO (23). However, the regulation of coronary vascular tone may be mediated, not only by NO, but also by the endothelium derived hyperpolarizing factor (EDHF) and adenosine (24). Yada et al. have demonstrated that endogenous  $\text{H}_2\text{O}_2$ , an EDHF, and rho-kinase inhibition mediated coronary vasodilation to a greater extent in arterioles than in small arteries (7, 8, 24). In the present study, preservation of endothelium-dependent vasodilation by edaravone was noted to a greater extent in the small arteries (Fig. 1). These facts revealed various mechanisms and 'site-specific' action of different drugs or agents in the coronary circulation. These also indicated a predominant role of NO in small arteries, as opposed to arterioles. Taken together, the

protective effects of NO and EDHF in coronary microvessels during I/R may occur in a compensatory manner.

Most of the NO production in the normal heart is accounted for by the presence of nitric-oxide synthase (eNOS) in the coronary endothelium and myocardium. Impaired NO synthesis from eNOS is a mechanism of endothelial dysfunction in the post-ischemic heart. The present study demonstrated reduced eNOS protein expression in the ischemic myocardium after I/R, whereas edaravone administration preserved the expression (Fig. 4). Previous studies from our institution have also demonstrated a decrease in eNOS protein expression in ischemic myocardium following I/R (7, 8). An *in vitro* study in HUVEC has shown that edaravone may increase eNOS expression via the inhibition of LDL oxidation (25). Thus, the burst of ROS generation during I/R may cause cell injury that results in reduced eNOS production, and edaravone administration preserves the eNOS expression.

#### *Myocardial protection by edaravone*

The present study confirmed the protective effect of edaravone on the myocardial cell (13) and revealed that the cardioprotective role of edaravone during I/R was irrespective of transmural collateral flow to the ischemic area (Fig. 5). It has been hypothesized that maintenance of endothelium-dependent dilation of coronary microvessels could enhance reperfusion damage and reduces the amount of tissue necrosis (26). Thus, preservation of microvascular endothelial function

by edaravone probably contributed to the improvement in myocardial perfusion, thereby facilitating myocardial tissue preservation after I/R.

In the present study, we administered edaravone prior to coronary occlusion because ROS generation may occur during occlusion and after reperfusion. Wu et al. have shown a protective effect of edaravone on the myocardium when it was administered during coronary occlusion or after reperfusion (27). Thus, we presumed that preservation of endothelial function by edaravone may also be observed if it is administered during occlusion or after reperfusion. Nevertheless, further study is needed to confirm these issues.

### Conclusions

In conclusion, edaravone exerts beneficial protective effects on coronary microvessels by preserving endothelial function after I/R *in vivo*. These effects are attributed to the ROS scavenging properties of edaravone and involves an NO-mediated mechanism.

### Acknowledgments

This work was supported in part by a grant (No.16300164) from the Japanese Ministry of Education, Science, Sports, Culture, and Technology and a grant from the program for promotion of fundamental studies in health sciences of the Organization for Pharmaceutical Safety and Research in Japan.

### References

- Chilian WM, Kuo L, DeFily DV, Jones CJ, Davis MJ. Endothelial regulation of coronary microvascular tone under physiological and pathophysiological conditions. *Eur Heart J*. 1993;1 Suppl 1:55-59.
- Kuo L, Davis MJ, Chilian WM. Endothelium-dependent, flow-induced dilation of isolated coronary arterioles. *Am J Physiol*. 1990;259:1063-1170.
- Suwaidi JA, Hamasaki S, Higano ST, Nishimura RA, Holmes DR, Lerman A. Long-term follow-up of patients with mild coronary artery disease and endothelial dysfunction. *Circulation*. 2000;101:948-954.
- Schächinger V, Britten B, Zeiher AM. Prognostic impact of coronary vasodilator dysfunction on adverse long-term outcome of coronary heart disease. *Circulation*. 2000;101:1899-1906.
- Targonski PV, Bonetti PO, Pumper GM, Higano ST, Holmes DR, Lerman A. Coronary endothelial dysfunction is associated with an increased risk of cerebrovascular events. *Circulation*. 2003;107:2805-2809.
- Matsumura K, Jeremy RW, Schaper J. Progression of myocardial necrosis during reperfusion of ischemic myocardium. *Circulation*. 1998;97:795-804.
- Yada T, Shimokawa H, Hiramatsu O, Kajita T, Shigeto F, Tanaka E, et al. Beneficial effect of hydroxyfasudil, a specific Rho-kinase inhibitor, on ischemia/reperfusion injury in canine coronary microcirculation *in vivo*. *J Am Coll Cardiol*. 2005;45:599-607.
- Yada T, Shimokawa H, Hiramatsu O, Haruna Y, Morita Y, Kashihara N, et al. Cardioprotective role of endogenous hydrogen peroxide during ischemia-reperfusion injury in canine coronary microcirculation *in vivo*. *Am J Physiol Heart Circ Physiol*. 2006;291:H1138-1146.
- Bolli R, Jeroudi MO, Patel BS, DuBose CM, Lai EK, Roberts R, et al. Direct evidence that oxygen-derived free radicals contribute to postischemic myocardial dysfunction in the intact dog. *Proc Natl Acad Sci U S A*. 1989;86:4695-4699.
- Zweier JL, Talukder MA. The role of oxidants and free radicals in reperfusion injury. *Cardiovasc Res*. 2006;70:181-190.
- Becker LB, vanden Hoek TL, Shao ZH, Li CQ, Schumacker PT. Generation of superoxide in cardiomyocytes during ischemia before reperfusion. *Am J Physiol*. 1999;277:H2240-H2246.
- Kevin LG, Camara AK, Riess ML, Novalija E, Stowe DF. Ischemic preconditioning alters real-time measure of O<sub>2</sub> radicals in intact hearts with ischemia and reperfusion. *Am J Physiol Heart Circ Physiol*. 2003;284:H566-H574.
- Yamawaki M, Sasaki N, Shimoyama M, Miake J, Ogino K, Igawa O, et al. Protective effect of edaravone against hypoxia-reoxygenation injury in rabbit cardiomyocytes. *Br J Pharmacol*. 2004;142:618-626.
- Shichinohe H, Kuroda S, Yasuda H, Ishikawa T, Iwai M, Horiuchi M. Neuroprotective effects of the free radical scavenger edaravone (MCI-186) in mice permanent focal brain ischemia. *Brain Res*. 2004;1029:200-206.
- Yada T, Hiramatsu O, Kimura A, Goto M, Ogasawara Y, Tsujioka K. *In vivo* observation of subendocardial microvessels of the beating porcine heart using a needle-probe video-microscope with a CCD camera. *Circ Res*. 1993;72:939-946.
- Satoh M, Fujimoto S, Haruna Y, Arakawa S, Horike H, Komai N, et al. NAD(P)H oxidase and uncoupled nitric oxide synthase are major sources of glomerular superoxide in rats with experimental diabetic nephropathy. *Am J Physiol Renal Physiol*. 2005;288:F1144-F1152.
- Mori H, Haruyama S, Shinozaki Y, Okino H, Iida A, Takanashi R, et al. New nonradioactive microspheres and more sensitive X-ray fluorescence to measure regional blood flow. *Am J Physiol Heart Circ Physiol*. 1992;263:H1946-H1957.
- Ogita H, Node K, Asanuma H, Sanada S, Takashima S, Asakura M. Amelioration of ischemia- and reperfusion-induced myocardial injury by the selective estrogen receptor modulator, raloxifene, in the canine heart. *J Am Coll Cardiol*. 2002;40:998-1005.
- Zhang N, Komine-Kobayashi M, Tanaka R, Liu M, Mizuno Y, Urabe T. Edaravone reduces early accumulation of oxidative products and sequential inflammatory responses after transient focal ischemia in mice brain. *Stroke*. 2005;36:2220-2225.
- Nimata M, Okabe TA, Hattori M, Yuan Z, Shioji K, Kishimoto C. MCI-186 (edaravone), a novel free radical scavenger, protects against acute autoimmune myocarditis in rats. *Am J Physiol Heart Circ Physiol*. 2005;289:H2514-H2518.
- Szocs K. Endothelial dysfunction and reactive oxygen species production in ischemia/reperfusion and nitrate tolerance. *Gen Physiol Biophys*. 2004;23:265-269.
- Jitsuiki D, Higashi Y, Goto C, Kimura M, Noma K, Hara K, et al. Effect of edaravone, a novel free radical scavenger, on

- endothelium-dependent vasodilation in smokers. *Am J Cardiol.* 2004;94:1070-10703.
- 23 Neishi Y, Mochizuki S, Miyasaka T, Kawamoto T, Kume T, Sukmawan R, et al. Evaluation of bioavailability of nitric oxide in coronary circulation by direct measurement of plasma nitric oxide concentration. *Proc Natl Acad Sci U S A.* 2005;102:11456-11461.
- 24 Yada T, Shimokawa H, Hiramatsu O, Kajita T, Shigeto F, Goto M, et al. Hydrogen peroxide, an endogenous endothelium-derived hyperpolarizing factor, plays an important role in coronary autoregulation in vivo. *Circulation.* 2003;107:1040-1045.
- 25 Yoshida H, Sasaki K, Namiki Y, Sato N, Tada N, Edaravone, a novel radical scavenger, inhibits oxidative modification of low-density lipoprotein (LDL) and reverses oxidized LDL-mediated reduction in the expression of endothelial nitric oxide synthase. *Atherosclerosis.* 2005;179:97-102.
- 26 DeFily DV, Chilian WM. Preconditioning protects coronary arteriolar endothelium from ischemia-reperfusion injury. *Am J Physiol.* 1993;265:H700-H706.
- 27 Wu TW, Zeng LH, Wu J, Fung KP. Myocardial protection of MCI-186 in rabbit ischemia-reperfusion. *Life Sci.* 2002;71:2249-2255.

# Crystal structure of RVV-X: An example of evolutionary gain of specificity by ADAM proteinases

Soichi Takeda\*, Tomoko Igarashi, Hidezo Mori

Department of Cardiac Physiology, National Cardiovascular Center Research Institute, 5-7-1 Fujishiro-dai, Suita, Osaka 565-8365, Japan

Received 2 November 2007; revised 21 November 2007; accepted 21 November 2007

Available online 3 December 2007

Edited by Hans Eklund

**Abstract** Russell's viper venom factor X activator (RVV-X) is a heterotrimeric metalloproteinase with a mammalian ADAM-like heavy chain and two lectin-like light chains. The crystal structure of RVV-X has been determined at 2.9 Å resolution and shows a hook-spanner-wrench-like architecture, in which the metalloproteinase/disintegrin region constitutes a hook, and the lectin-like domains constitute a handle. A 6.5 nm separation between the catalytic site and a putative exosite suggests a docking model for factor X. The structure provides a typical example of the molecular evolution of multi-subunit proteins and insights into the molecular basis of target recognition and proteolysis by ADAM/adamalysin/reprolysin proteinases.  
© 2007 Federation of European Biochemical Societies. Published by Elsevier B.V. All rights reserved.

**Keywords:** Metalloproteinase; Disintegrin; ADAM; Factor X activator; Snake venom; Reprolysin

## 1. Introduction

Blood coagulation factor X is a serine proteinase and is one of the key components of the hemostatic system [1]. In circulation, factor X exists as a zymogen and is converted to an active form, factor Xa, by cleavage of a single peptide bond between Arg194 and Ile195. This removes the heavily glycosylated first 52 amino terminal residues (AP: active peptide) of the heavy chain, resulting in exposure of the active site. Factor Xa in turn converts prothrombin to thrombin, which ultimately leads to formation of hemostatic plugs.

Venom from Russell's viper, *Daboia russelli*, has been recognized for its potent coagulation activity. Russell's viper venom factor X activator (RVV-X) is a well-characterized metalloproteinase which specifically activates factor X by cleaving the same Arg-Ile bond in factor X that is cleaved by factors IXa and VIIa during physiological coagulation [2,3]. RVV-X belongs to the P-IV class of snake venom metalloproteinases [4] and consists of a heavy chain of 57,600 Da and two light chains of 19,400 and 16,400 Da, linked by disulfide bonds [2,5,6]. The 427-residue heavy chain contains the metallopro-

teinase (M)/disintegrin (D)/cysteine-rich (C) domains [4,7] that are shared by the (ADAM) (a disintegrin and metalloproteinase)/adamalysin/reprolysin family proteins. ADAMs are membrane-anchored glycoproteins that can proteolytically release cell-surface-protein ectodomains, including cell adhesion molecules, growth factor precursors and their receptors, and have been associated with numerous diseases including rheumatoid arthritis, Alzheimer's disease, heart disease, and cancer [8,9]. The light chains of RVV-X share amino acid sequence homology with mammalian C-type (Ca<sup>2+</sup>-dependent) lectins and C-type lectin-like proteins (CLPs) isolated from various snake venoms [7,10]. RVV-X is one of the best examples of an exogenous activators used in coagulation research and has also been frequently used in diagnostic applications [2]. However, the molecular mechanism by which RVV-X recognizes and cleaves factor X is poorly understood, primarily due to the lack of three-dimensional structural information.

We recently determined the three-dimensional structure of the metalloproteinase/disintegrin/cysteine-rich (MDC) domains of ADAM/adamalysin/reprolysin family protein VAP1 and suggested a potential protein-protein interaction site that may function in specifying target proteins [11]. Among the family proteins, RVV-X is unique in having CLP domains within the molecule and a strict substrate specificity. To extend our understanding of the protein-protein interactions and target specificity of this family of proteins, we determined the crystal structure of RVV-X. Here, we report the crystal structure of RVV-X at 2.9 Å resolution and present a factor X docking model.

## 2. Materials and methods

RVV-X was purchased from Enzyme Research Laboratories Inc. and was further purified using a CM Hi-Trap column (GE healthcare Bio-Science Corp.) in the presence of GM6001 (*N*-(2*R*)-2-(hydroxamidocarbonyl)ethyl)-4-methylpentanoyl-L-tryptophan methylamide (CALBIOCHEM)). Crystals were obtained by the sitting drop vapor diffusion method. Droplets were prepared by mixing 1 µl of protein solution and 1 µl of reservoir solution (0.1 M calcium acetate, 0.1 M sodium cacodylate, 10% PEG8000, pH 6.5) supplemented with one fifth volume of 10% PEG3350 and were equilibrated against 1 ml of reservoir solution at 293 K, typically for one week. Crystals were soaked in reservoir solution supplemented with 15% MPD (2-methyl-2,4-pentandiol) prior to flash cryo-cooling under a stream of nitrogen gas at 100 K.

The diffraction data set was acquired using the SPring-8 beamline BL41XU at a wavelength of 1.0 Å at 100 K. The best crystal generated a data set with a 2.9 Å resolution (Table 1). The asymmetric unit contained one RVV-X molecule. The RVV-X structure was solved by the molecular replacement method using search models constructed from acutolysin-C (1QUA), catrocollastatin/VAP2B (2DW0), and fIX-bind-

\*Corresponding author. Fax: +81 6 6872 7485.  
E-mail address: stakeda@ri.nccvc.go.jp (S. Takeda).

**Abbreviations:** RVV-X, Russell's viper venom factor X activator; ADAM, a disintegrin and metalloproteinase; MDC, metalloproteinase/disintegrin/cysteine-rich; HVR, hyper-variable-region; PEG, polyethyleneglycol

Table 1  
Data collection and refinement statistics

	Crystal 1
<b>Data collection</b>	
Space group	P2 <sub>1</sub> 2 <sub>1</sub> 2 <sub>1</sub>
Cell dimensions	
<i>a</i> , <i>b</i> , <i>c</i> (Å)	70.4, 91.7, 152.9
$\alpha$ , $\beta$ , $\gamma$ (°)	90, 90, 90
Resolution (Å)	50–2.9 (3.0–2.9)
<i>R</i> <sub>merge</sub> <sup>a</sup>	0.069 (0.212)
<i>I</i> / $\sigma$ <i>I</i>	17.0 (7.0)
Completeness (%)	96.4 (79.5)
Redundancy	6.3 (5.5)
<b>Refinement</b>	
Resolution (Å)	44.6–2.91 (3.0–2.91)
No. reflections	21482 (1661)
<i>R</i> <sub>work</sub> <sup>b</sup> / <i>R</i> <sub>free</sub> <sup>c</sup>	0.218/0.273
No. atoms	
Protein	5300
Zn <sup>2+</sup>	1
Ca <sup>2+</sup>	5
carbohydrate	106
GM6001	28
R.m.s deviations	
Bond lengths (Å)	0.0045
Bond angles (°)	1.12

Highest resolution shell is shown in parenthesis.

<sup>a</sup> $R_{\text{merge}} = \frac{\sum_{hkl} \sum_i |I_i(hkl) - \langle I(hkl) \rangle|}{\sum_{hkl} \sum_i I_i(hkl)}$ , where  $I_i(hkl)$  is the *i*th intensity measurement of reflection *hkl* and  $\langle I(hkl) \rangle$  is its average.

<sup>b</sup> $R_{\text{work}} = \frac{\sum (||F_{\text{obs}}| - |F_{\text{calc}}||)}{\sum |F_{\text{obs}}|}$ .

<sup>c</sup> $R_{\text{free}} = R$ -value for a randomly selected subset (5%) of the data that were not used for minimization of the crystallographic residual.

ing protein (IX-bp, 1J34), for the M, C and CLP domains, respectively. The final model includes amino acid residues 7–422 of the heavy chain, 1–59 and 64–133 of light chain-A (LA) and 3–123 of light chain-B (LB), and was refined to a resolution of 2.9 Å (Table 1). The overall resolution is not particularly high when compared to those of the other snake venom protein structures, most likely due to the relatively high solvent content of the crystal (~60%) and the flexible modular architecture of the MDC domains [12]. However, well-determined structural models for most sub-domains generated the electron-density maps that enable us to build a reliable model. The overall B-factor is relatively high (average B-factor of the total protein atoms is 72.2 Å<sup>2</sup>) and the electron-densities associated with the charged side-chains located on the molecular surface (61 aa corresponding to 9% of the total model of 672 aa) are not clearly observed, however, almost all of the side-chains inside the molecule are defined in the final electron-density maps (Fig. 1B and C). Details of preparation, crystallization and structural analysis are described in the Supplementary information.

### 3. Results and discussion

#### 3.1. Overall structure of RVV-X

The overall structure of RVV-X resembles a hook-spanner-wrench configuration, where the major portion of the heavy chain forms a hook and the remaining heavy chain portion and the light chains form a handle (Fig. 1A). The backbone structure of the heavy chain is essentially the same as each monomer of VAP1 [11] and catrocollastain/VAP2B [12], with the exception of the sub-domain orientations (Fig. 1D and E). There are direct, but less-specific interactions between the M and C domains, most likely resulting from crystal packing forces, such that the entire RVV-X MDC domain forms a closed C-shape structure, unlike the open C-shaped structures of VAP1 and catrocollastain/VAP2B. The M domain of RVV-X has a flat elliptical shape with a core formed by a five-

stranded  $\beta$ -sheet and five  $\alpha$ -helices and contains the conserved Zn<sup>2+</sup>-binding HEXXHXXGXXHD sequence (residues 145–156) and a “Met-tern” (Met169) bearing the typical structural features of the metzincin family of metalloproteinases [13]. RVV-X has a fourth disulfide bridge (Cys27–Cys63) (Fig. 1B), in addition to the three conserved disulfide bridges (Cys120–Cys200, Cys160–Cys184 and Cys162–Cys167) [4] in the M domain. The M domain is followed by the D and C domains, which are further divided into shoulder (D<sub>s</sub>), arm (D<sub>a</sub>), wrist (C<sub>w</sub>) and hand (C<sub>h</sub>), segments, and the entire heavy chain folds into a C-shaped structure (Fig. 1A). The heavy chain contains three structural Ca<sup>2+</sup>-binding sites and a number of disulfide bridges (9 and 5 in the D and C domains, respectively) that are highly conserved among the ADAM/adamalysin/reprolysin family proteins [11,12].

The two homologous light chains have a fold similar to the carbohydrate-recognition domain (CRD) of rat mannose binding protein (MBP) [14], but they form an intertwined dimer where the central portion of each chain projects toward the adjoining subunit (Fig. 1A). The light chains are related by a pseudo 2-fold axis which is perpendicular to the long axis of the light chain dimer.

#### 3.2. (HVR)-mediated protein–protein interaction

RVV-X has a unique cysteine residue (Cys389) in the middle of the hyper-variable-region (HVR, residues 373–394) in C<sub>h</sub>, a putative protein–protein interaction site for this family of proteins [11]. Cys389 forms a disulfide bond with the C-terminal cysteine residue (Cys133) of LA (Fig. 1A and C). Aside from this inter-chain disulfide bridge, Tyr346, Tyr347, and Met385 in the heavy chain form multiple hydrophobic interactions and hydrogen bonds with Tyr11, Phe12, and Pro131 in LA, which further stabilize the continuous C<sub>h</sub>/LA structure (Fig. 1C). Most of these residues involved in the interaction between C<sub>h</sub> and LA are not conserved among ADAMs [11,12] or among other CLPs [10]. The RVV-X structure represents the first example of HVR-mediated protein–protein interactions by the ADAM/adamalysin/reprolysin family proteins.

#### 3.3. Light chains

Both the overall structure and the surface features of the RVV-X light chains are quite similar to those of the factor X-binding protein (X-bp) from *Deinagkistrodon actus* venom (the r.m.s. deviation of the 240 equivalent C $\alpha$  atoms is 2.6 Å) determined in complex with the  $\gamma$ -carboxyglutamic acid (Gla) domain of factor X [15] (Fig. 2A and B). X-bp has strong anticoagulant activities because it binds to the Gla domain of factor X and inhibits its membrane-anchoring function [16]. The hydrophobic residues that are critical for the membrane-anchoring function of factor X (Phe4, Leu5 and Val8) interact with the hydrophobic patch formed by the hydrophobic residues (Met113, Ile114 and Ala115) of the B chain in X-bp [15]. Those residues are conserved in RVV-X (Phe114, Ile115 and Ala116 of LB) (Fig. 2B). The positively charged patches on X-bp that directly interact with the Gla residues in factor X are conserved, but, are less prominent in RVV-X because of amino acid substitutions (especially, Ile101 and Glu104) (Fig. 2B). The structural similarities between the RVV-X light chains and X-bp suggest the intriguing possibility that RVV-X recognizes the factor X Gla domain through an exosite, formed by the light chains (Fig. 2C).

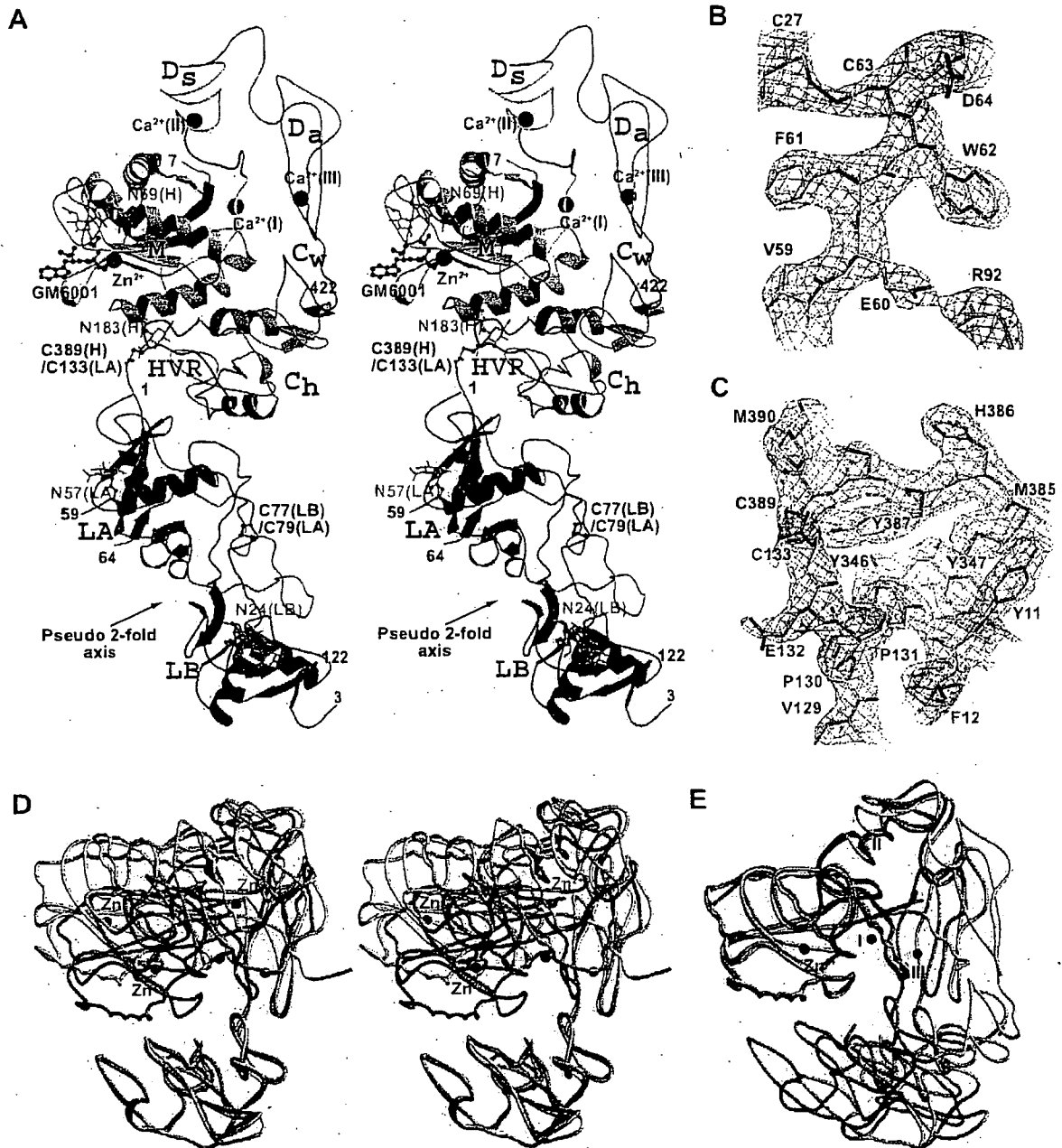


Fig. 1. Structure of RVV-X. (A) Ribbon structure of RVV-X in stereo. Bound calcium and zinc ions are represented by black and red spheres, respectively. The carbohydrate moieties (in green) linked to asparagine residues and GM6001 (in magenta) are shown in ball-and-stick representations.  $2F_o - F_c$  electron-density maps ( $1.0\sigma$ ) around the disulfide bridge between Cys27(HC) and Cys63(HC), and between Cys389(HC) and Cys133(LA) are represented in (B) and in (C), respectively. The HC and LA residues are labelled in black and in red, respectively. (D) Superimposition of the C<sub>1</sub> segment of the RVV-X heavy chain (in pink) with that of the VAP1 monomer (chain-A in 2ERO, in yellow), and with that of the catrocollastatin/VAP2B (chain-A in 2DW0, in cyan) in stereo. The bound zinc and calcium atoms in RVV-X are shown as red and black spheres, respectively. The zinc atoms in VAP1 and catrocollastatin/VAP2B are shown as green and blue spheres, respectively. (E) Superimposition of the M domain of the RVV-X heavy chain with the M domains of the VAP1 monomer and catrocollastatin/VAP2B.

When a properly folded Gla domain is absent from factor X, the rate of factor X activation by RVV-X is markedly diminished. In the acarboxy factor X, in which Gla formation has been blocked by a vitamin K antagonist [17] or the Des (1-44) factor X [18], factor X activation occurs at less than 1% of the rate of native factor X. Activation of factor X by RVV-X is dra-

matically enhanced by millimolar  $Ca^{2+}$ , which induces a conformational change in the Gla domain that enhances its binding to RVV-X [19]. Moreover, RVV-X catalyzed factor X activation is inhibited by X-bp [7]. Collectively, these observations suggest that the concave cleft created between the two light chains in RVV-X may function as an exosite for factor X-binding.

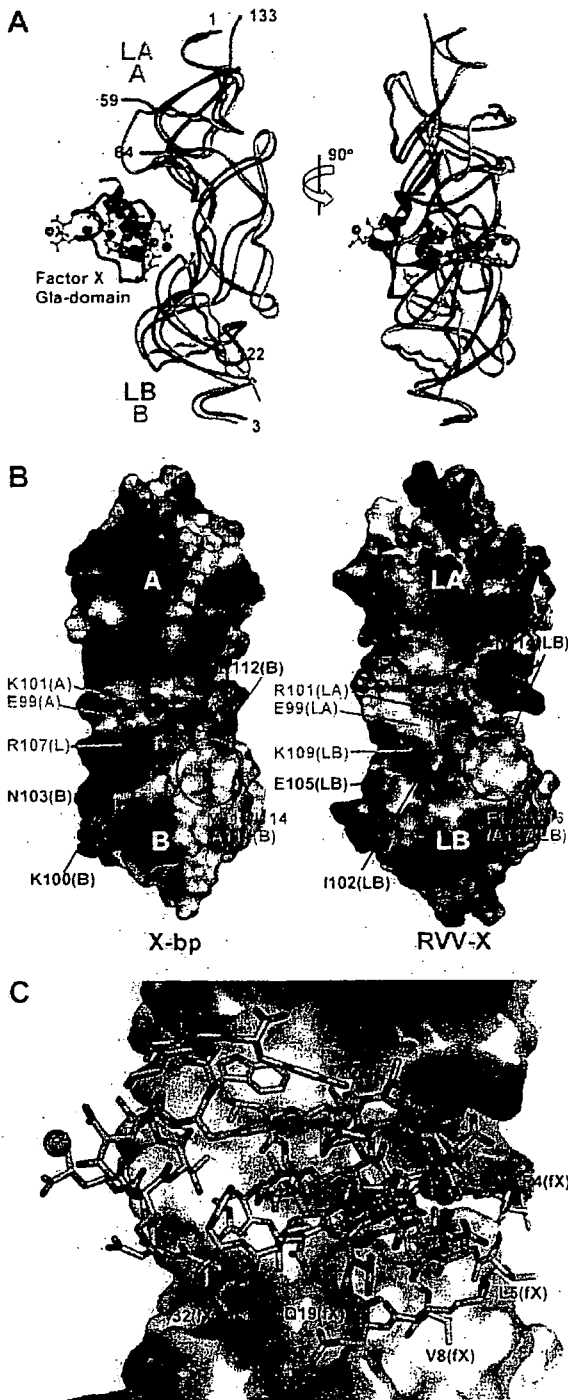


Fig. 2. Comparison of the RVV-X light chains and X-bp. (A) Superimposition of the RVV-X light chains (LA in orange and LB in magenta) onto the structure of X-bp (in gray) in complex with the Gla domain (in pink) of factor Xa (1IOD). The Gla residues and the  $Ca^{2+}$  ions are shown in ball-and-stick representation and as green spheres, respectively. (B) The molecular surfaces of X-bp and the light chains of RVV-X are represented according to their electrochemical potentials (blue for positive, red for negative) and are viewed from the pseudo 2-fold axis. Conserved and varied residues are labelled in cyan and in red, respectively. (C) A model of the RVV-X light chains in complex with the Gla domain that was positioned based on the X-bp/fX Gla domain complex structure.

3.4. Docking model

Fig. 3A represents a preliminary docking model. For constructing a model, firstly, the second EGF domain (EGF2) and the serine proteinase (SP) domain of factor Xa (PDBID:1XKA) were placed such that the N-terminus of the factor X heavy chain (Ile195) closely approaches the RVV-X active site, and the globular SP domain fits into the concave

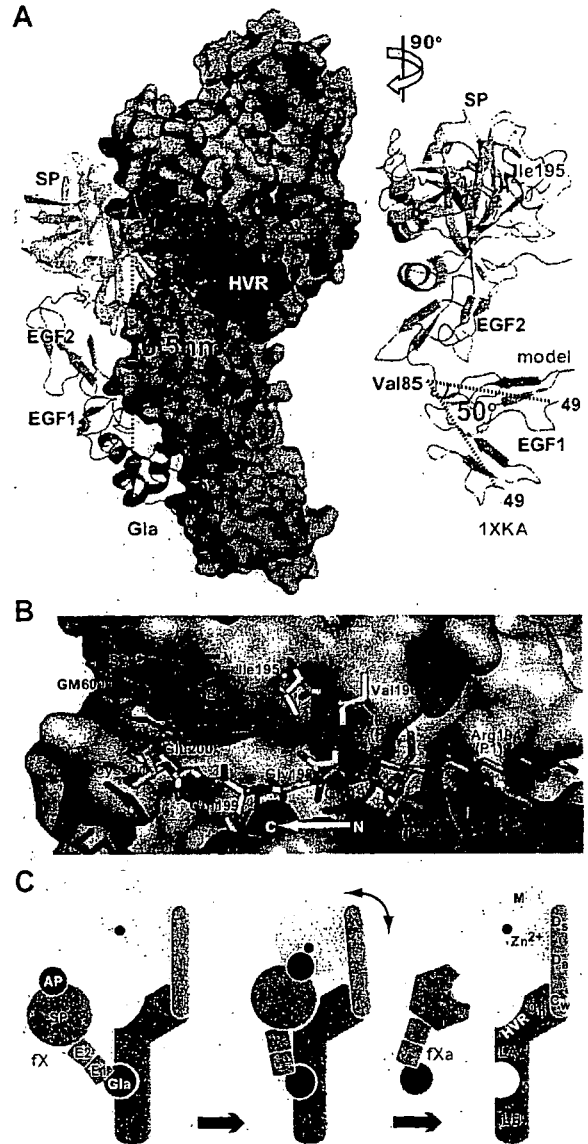


Fig. 3. Docking model. (A) The surfaces of the RVV-X sub-domains are coloured as in Fig. 1A. Factor Xa is shown in ribbon representation. Ile195 (in stick representation) and the N-terminal region (residues 195–201) of the factor X heavy chain are shown in magenta. In the right panel, the EGF1 segment of the original structural model (1XKA) is shown in gray. (B) Close up view of the RVV-X catalytic site of the docking model viewed from inside the factor Xa molecule. The N-terminal residues of factor Xa are shown in white and those of the model of factor X (zymogen) are shown in light pink. Because the factor X structure is currently unavailable, we assumed that this region has an extended structure. (C) Schematic model of factor X activation by RVV-X.

surface created by the C<sub>1</sub>/LA domains. Secondly, we introduced a 50° bend between the two EGF domains so that the EGF1 domain fits to the convex surface of the LA domain (Fig. 3A). The linker between the two EGF domains is most likely flexible in solution [20]. This displacement successfully placed the N-terminus of the EGF1 domain in close proximity to the C-terminus of the Gla domain.

In the factor Xa structure, the N-terminal residue of the heavy chain, Ile195, is buried within the protein [20]. However, in the zymogen, the intact Arg194-Ile195-containing segment must be situated on the molecular surface, as in the equivalent segments of other serine proteinase zymogen structures [21]. The region of factor X that is C-terminal to the scissile peptide (segment coloured in magenta in Fig. 3A) may be located along the surface of the SP domain, resulting in its binding to the primed region of RVV-X, in the same orientation as the peptide-like inhibitor GM6001 lies in the current crystal structure (Fig. 3B). In the present docking model, since both molecules were positioned just as a rigid body without any collision, the active site zinc atom of RVV-X and Ile195 of factor Xa are 16 Å apart. Intrinsic hinge motions of the modular M/D<sub>1</sub>/D<sub>2</sub>/C<sub>w</sub> architecture [12], and conformational changes upon association of RVV-X and the factor X zymogen, may allow the catalytic site of RVV-X to interact directly with the Arg194-Ile195 bond of factor X when in solution (Fig. 3C). The relatively large separation (~65 Å) of the catalytic site and the Gla-domain-binding exosite may explain the high specificity of RVV-X for factor X.

### 3.5. Implication for molecular evolution of RVV-X

CLPs from snake venoms are characterized by a unique dimerization mechanism of protein evolution, in which two monomers swap a portion of the long loop region, forming a stable functional unit and creating a new concave surface for target binding for a variety of biological activities [10]. Dimers can further aggregate with each other to form higher-order oligomers [22], or, as in the case of RVV-X, form covalently linked complexes with a metalloproteinase chain creating an exosite. The RVV-X structure illustrates a good example of evolutionary gain of function by multi-subunit proteins, represented by the fold adaptation, for the binding of other ligands.

## 4. Conclusion

ADAMs are widely distributed and constitute the major membrane-bound sheddases to play roles in important processes occurring at the cell surface. However, the molecular mechanism of target recognition by ADAMs and which ADAMs shed which key substrates in specific biological events has been poorly understood. Previously, we suggested that the HVR may constitute an exosite that captures the target or associated proteins, and that is processed by the catalytic site [11]. The RVV-X structure is consistent with this model and provides insights into the molecular basis of HVR-mediated protein-protein interactions and target recognition by ADAM/adamalsin/reprolysin family proteins.

**Acknowledgements:** The authors thank M. Tomisako for help in crystallization experiments, M. Kawamoto and N. Shimizu for assistance with data acquisition at the SPring-8 beamline BL41XU and T. Morita for helpful discussions. This work was partly supported by the Minis-

try of Education, Science, Sports and Culture. Grant-in-aid for Scientific Research B-19370047-2007, and Health and Labor Science Research Grants, and by grants from the Mitsubishi Pharma Research Foundation and the Astellas Foundation for Research on Metabolic Disorders. T.I is supported by the grant from New Energy and Industrial Technology Development Organization (NEDO) of Japan.

## Appendix A. Supplementary data

The atomic coordinates and structure factors have been deposited in the NCBI protein data bank with the accession code 2E3X. Supplementary data associated with this article can be found, in the online version, at doi:10.1016/j.febslet.2007.11.062.

## References

- [1] Mann, K.G., Nesheim, M.E., Church, W.R., Haley, P. and Krishnaswamy, S. (1990) Surface-dependent reactions of the vitamin K-dependent enzyme complexes. *Blood* 76, 1–16.
- [2] Morita, T. (1998) Proteases which activate factor X in: *Enzymes from Snake Venom* (Bailey, G.S., Ed.), pp. 179–208. Alaken, Colorado.
- [3] Tans, G. and Rosing, J. (2001) Snake venom activators of factor X: an overview. *Haemostasis* 31, 225–233.
- [4] Fox, J.W. and Serrano, S.M. (2005) Structural considerations of the snake venom metalloproteinases, key members of the M12 reprolysin family of metalloproteinases. *Toxicon* 45, 969–985.
- [5] Gowda, D.C., Jackson, C.M., Hensley, P. and Davidson, E.A. (1994) Factor X-activating glycoprotein of Russell's viper venom. Polypeptide composition and characterization of the carbohydrate moieties. *J. Biol. Chem.* 269, 10644–10650.
- [6] Kisiel, W., Hermodson, M.A. and Davie, E.W. (1976) Factor X activating enzyme from Russell's viper venom: isolation and characterization. *Biochemistry* 15, 4901–4906.
- [7] Takeya, H., Nishida, S., Miyata, T., Kawada, S., Saisaka, Y., Morita, T. and Iwanaga, S. (1992) Coagulation factor X activating enzyme from Russell's viper venom (RVV-X). A novel metalloproteinase with disintegrin (platelet aggregation inhibitor)-like and C-type lectin-like domains. *J. Biol. Chem.* 267, 14109–14117.
- [8] White, J.M. (2003) ADAMs: modulators of cell-cell and cell-matrix interactions. *Curr. Opin. Cell Biol.* 15, 598–606.
- [9] Seals, D.F. and Courtneidge, S.A. (2003) The ADAMs family of metalloproteases: multidomain proteins with multiple functions. *Genes Dev.* 17, 7–30.
- [10] Morita, T. (2005) Structures and functions of snake venom CLPs (C-type lectin-like proteins) with anticoagulant-, procoagulant-, and platelet-modulating activities. *Toxicon* 45, 1099–1114.
- [11] Takeda, S., Igarashi, T., Mori, H. and Araki, S. (2006) Crystal structures of VAP1 reveal ADAMs' MDC domain architecture and its unique C-shaped scaffold. *EMBO J.* 25, 2388–2396.
- [12] Igarashi, T., Araki, S., Mori, H. and Takeda, S. (2007) Crystal structures of catrocollastatin/VAP2B reveal a dynamic, modular architecture of ADAM/adamalsin/reprolysin family proteins. *FEBS Lett.* 581, 2416–2422.
- [13] Gomis-Ruth, F.X. (2003) Structural aspects of the metzincin clan of metalloendopeptidases. *Mol. Biotechnol.* 24, 157–202.
- [14] Weis, W.I., Kahn, R., Fourme, R., Drickamer, K. and Hendrickson, W.A. (1991) Structure of the calcium-dependent lectin domain from a rat mannose-binding protein determined by MAD phasing. *Science* 254, 1608–1615.
- [15] Mizuno, H., Fujimoto, Z., Atoda, H. and Morita, T. (2001) Crystal structure of an anticoagulant protein in complex with the Gla domain of factor X. *Proc. Natl. Acad. Sci. USA* 98, 7230–7234.
- [16] Atoda, H., Ishikawa, M., Mizuno, H. and Morita, T. (1998) Coagulation factor X-binding protein from Deinagkistrodon acutus venom is a Gla domain-binding protein. *Biochemistry* 37, 17361–17370.



- [17] Lindhout, M.J., Kop-Klaassen, B.H. and Hemker, H.C. (1978) Activation of decarboxyfactor X by a protein from Russell's viper venom. Purification and partial characterization of activated decarboxyfactor X. *Biochim. Biophys. Acta* 533, 327–341.
- [18] Morita, T. and Jackson, C.M. (1986) Preparation and properties of derivatives of bovine factor X and factor Xa from which the gamma-carboxyglutamic acid containing domain has been removed. *J. Biol. Chem.* 261, 4015–4023.
- [19] Skogen, W.F., Bushong, D.S., Johnson, A.E. and Cox, A.C. (1983) The role of the Gla domain in the activation of bovine coagulation factor X by the snake venom protein XCP. *Biochem. Biophys. Res. Commun.* 111, 14–20.
- [20] Kamata, K., Kawamoto, H., Honma, T., Iwama, T. and Kim, S.H. (1998) Structural basis for chemical inhibition of human blood coagulation factor Xa. *Proc. Natl. Acad. Sci. USA* 95, 6630–6635.
- [21] Freer, S.T., Kraut, J., Robertus, J.D., Wright, H.T. and Xuong, N.H. (1970) Chymotrypsinogen: 2.5-angstrom crystal structure, comparison with alpha-chymotrypsin, and implications for zymogen activation. *Biochemistry* 9, 1997–2009.
- [22] Fukuda, K., Mizuno, H., Atoda, H. and Morita, T. (2000) Crystal structure of flavocetin-A, a platelet glycoprotein Ib-binding protein, reveals a novel cyclic tetramer of C-type lectin-like heterodimers. *Biochemistry* 39, 1915–1923.

PRECLINICAL STUDIES

## Important Role of Endogenous Hydrogen Peroxide in Pacing-Induced Metabolic Coronary Vasodilation in Dogs In Vivo

Toyotaka Yada, MD, PhD,\* Hiroaki Shimokawa, MD, PhD,† Osamu Hiramatsu, PhD,\*  
Yoshiro Shinozaki, BS,‡ Hidezo Mori, MD, PhD,§ Masami Goto, MD, PhD,\*  
Yasuo Ogasawara, PhD,\* Fumihiko Kajiya, MD, PhD\*  
*Kurashiki, Sendai, Isehara, and Suita, Japan*

<b>Objectives</b>	We examined whether endogenous hydrogen peroxide ( $H_2O_2$ ) is involved in pacing-induced metabolic vasodilation in vivo.
<b>Background</b>	We have previously demonstrated that endothelium-derived $H_2O_2$ is an endothelium-derived hyperpolarizing factor in canine coronary microcirculation in vivo. However, the role of endogenous $H_2O_2$ in metabolic coronary vasodilation in vivo remains to be examined.
<b>Methods</b>	Canine subepicardial small coronary arteries ( $\geq 100 \mu m$ ) and arterioles ( $< 100 \mu m$ ) were continuously observed by a microscope under cyclooxygenase blockade (ibuprofen, 12.5 mg/kg intravenous [IV]) (n = 60). Experiments were performed during paired right ventricular pacing under the following 7 conditions: control, nitric oxide (NO) synthase inhibitor ( $N^G$ -monomethyl-L-arginine [L-NMMA], 2 $\mu mol/min$ for 20 min intracoronary [IC]), catalase (a decomposer of $H_2O_2$ , 40,000 U/kg IV and 240,000 U/kg/min for 10 min IC), 8-sulfophenyltheophylline (SPT) (an adenosine receptor blocker, 25 $\mu g/kg/min$ for 5 min IC), L-NMMA+catalase, L-NMMA+tetraethylammonium (TEA) ( $K_{Ca}$ -channel blocker, 10 $\mu g/kg/min$ for 10 min IC), and L-NMMA+catalase+8-SPT.
<b>Results</b>	Cardiac tachypacing (60 to 120 beats/min) caused coronary vasodilation in both-sized arteries under control conditions in response to the increase in myocardial oxygen consumption. The metabolic coronary vasodilation was decreased after L-NMMA in subepicardial small arteries with an increased fluorescent $H_2O_2$ production compared with catalase group, whereas catalase decreased the vasodilation of arterioles with an increased fluorescent NO production compared with the L-NMMA group, and 8-SPT also decreased the vasodilation of arterioles. Furthermore, the metabolic coronary vasodilation was markedly attenuated after L-NMMA+catalase, L-NMMA+TEA, and L-NMMA+catalase+8-SPT in both-sized arteries.
<b>Conclusions</b>	These results indicate that endogenous $H_2O_2$ plays an important role in pacing-induced metabolic coronary vasodilation in vivo. (J Am Coll Cardiol 2007;50:1272-8) © 2007 by the American College of Cardiology Foundation

Cardiac tachycardia by pacing or exercise increases myocardial oxygen consumption ( $MVO_2$ ) and increases coronary blood flow by several mechanisms (1-3). Shear stress plays a crucial role in modulating vascular tone by endothelium-derived releasing factors (EDRFs), including nitric oxide (NO), prostacyclin ( $PGI_2$ ), and endothelium-derived hyperpolarizing factor (EDHF) (4,5). Flow-induced vasodilation is mediated by either NO (6,7),  $PGI_2$  (8), both of them

(9), or EDHF (10). Matoba et al. have previously identified that endothelium-derived hydrogen peroxide ( $H_2O_2$ ) is a

See page 1279

primary EDHF in mesenteric arteries of mice and humans (11,12). Morikawa et al. (13,14) subsequently confirmed

From the \*Department of Medical Engineering and Systems Cardiology, Kawasaki Medical School, Kurashiki, Japan; †Department of Cardiovascular Medicine, Tohoku University Graduate School of Medicine, Sendai, Japan; ‡Department of Physiology, Tokai University School of Medicine, Isehara, Japan; and the §Department of Cardiac Physiology, National Cardiovascular Center Research Institute, Suita, Japan. Dr. Yada is the winner of the Endothelium-Derived Hyperpolarizing Factor (EDHF) Tanabe Award from the Scientific Sessions of the American Heart Association,

November 2005, Dallas, Texas. This work was supported in part by grants from the Japanese Ministry of Education, Science, Sports, Culture, and Technology, Tokyo, Japan, Nos. 16209027 (to Dr. Shimokawa) and 16300164 (to Dr. Yada), the Program for Promotion of Fundamental Studies in Health Sciences of the Organization for Pharmaceutical Safety and Research of Japan (to Dr. Shimokawa), and Takeda Science Foundation 2002 (to Dr. Yada).

Manuscript received September 11, 2006; revised manuscript received April 25, 2007, accepted May 1, 2007.

that endothelial Cu,Zn-superoxide dismutase (SOD) plays an important role as an EDHF synthase in mice and humans. Miura et al. (15) demonstrated that endothelium-derived H<sub>2</sub>O<sub>2</sub> is involved as an EDHF in the flow-induced vasodilation of isolated human coronary arterioles in vitro. We have recently confirmed that endogenous H<sub>2</sub>O<sub>2</sub> plays an important compensatory role during coronary autoregulation (16) and reperfusion injury in vivo (17) through the interactions with NO and adenosine.

It is known that vascular  $\alpha$ -adrenergic receptor is modulated by the endothelium in dogs (18), whereas cardiac  $\beta$ -adrenergic receptor is modulated by K<sub>Ca</sub> channels in pigs (19) and H<sub>2</sub>O<sub>2</sub> in mice (20). However, the role of endogenous H<sub>2</sub>O<sub>2</sub> in metabolic coronary vasodilation in vivo remains largely unknown. In the present study, we thus examined whether H<sub>2</sub>O<sub>2</sub> is involved in pacing-induced metabolic coronary vasodilation in canine coronary microcirculation in vivo.

## Methods

This study conformed to the Guideline on Animal Experiments of Kawasaki Medical School and the Guide for the Care and Use of Laboratory Animals published by the U.S. National Institutes of Health.

**Animal preparation.** Anesthetized mongrel dogs of either gender (15 to 25 kg in body weight, n = 60) were ventilated with a ventilator (Model VS600, IDC, Pittsburgh, Pennsylvania). We continuously monitored aortic pressure and left ventricular pressure (LVP) with a catheter (SPC-784A, Millar, Houston, Texas) and blood flow of the left anterior descending coronary artery (LAD) with a transonic flow probe (T206, Transonic Systems, Ithaca, New York).

**Measurements of coronary diameter by intravital microscope.** We continuously monitored coronary vascular responses by an intravital microscope (VMS 1210, Nihon Kohden, Tokyo, Japan) with a needle-probe in vivo, as previously described (21). We gently placed the needle-probe on subepicardial microvessels. When a clear vascular image was obtained, end-diastolic vascular images were taken with 30 pictures/s (21).

**Measurements of regional myocardial blood flow.** Regional myocardial blood flow was measured by the non-radioactive microsphere (Sekisui Plastic Co. Ltd., Tokyo, Japan) technique, as previously described (22). Briefly, the microspheres suspension was injected into the left atrium 3 min after tachypacing. Myocardial flow in the LAD area was calculated according to the formula "time flow = tissue counts  $\times$  (reference flow/reference counts)" and was expressed in ml/g/min (22).

**Detection of H<sub>2</sub>O<sub>2</sub> and NO production in coronary microvessels.** 2',7'-dichlorodihydrofluorescein diacetate (DCF) (Molecular Probes, Eugene, Oregon) and diaminorhodamine-4M AM (DAR) (Daiichi Pure Chemicals, Tokyo, Japan) were used to detect H<sub>2</sub>O<sub>2</sub> and NO production in coronary microvessels, respectively, as previ-

ously described (17). Briefly, fresh and unfixed heart tissues were cut into several blocks and immediately frozen in optimal cutting temperature compound (Tissue-Tek, Sakura Fine Chemical, Tokyo, Japan). Fluorescent images of the microvessels were obtained 3 min after application of acetylcholine (ACh) by using a fluorescence microscope (OLYMPUS BX51, Tokyo, Japan) (17).

**Experimental protocols.** After the surgical procedure and instrumentation, at least 30 min were allowed for stabilization while monitoring hemodynamic variables. Coronary vasodilator responses were examined before and after cardiac tachypacing (60 to 120 beats/min) under the following 7 conditions with cyclooxygenase blockade (ibuprofen, 12.5 mg/kg, IV) to evaluate the role of H<sub>2</sub>O<sub>2</sub> and NO without PGI<sub>2</sub> in a different set of animals (Fig. 1): 1) control conditions without any inhibitor; 2) L-NMMA alone (2  $\mu$ mol/min intracoronary [IC] for 20 min); 3) catalase alone (40,000 U/kg intravenous [IV] and 240,000 U/kg/min IC for 10 min, an enzyme that dismutates

### Abbreviations and Acronyms

- CBF = coronary blood flow
- DAR = diaminorhodamine-4M AM
- DCF = 2',7'-dichlorodihydrofluorescein diacetate
- EDHF = endothelium-derived hyperpolarizing factor
- H<sub>2</sub>O<sub>2</sub> = hydrogen peroxide
- L-NMMA = N<sup>G</sup>-monomethyl-L-arginine
- LAD = left anterior descending coronary artery
- MVO<sub>2</sub> = myocardial oxygen consumption
- NO = nitric oxide
- PGI<sub>2</sub> = prostacyclin
- SPT = sulfophenyltheophylline
- TEA = tetraethylammonium

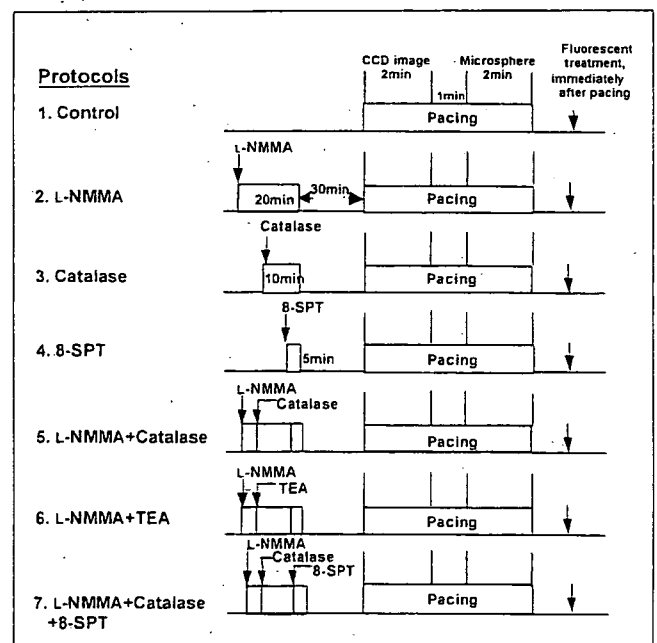


**Figure 1** Experimental Protocols

CCD = charge-coupled device; L-NMMA = N<sup>G</sup>-monomethyl-L-arginine; SPT = sulfophenyltheophylline; TEA = tetraethylammonium.

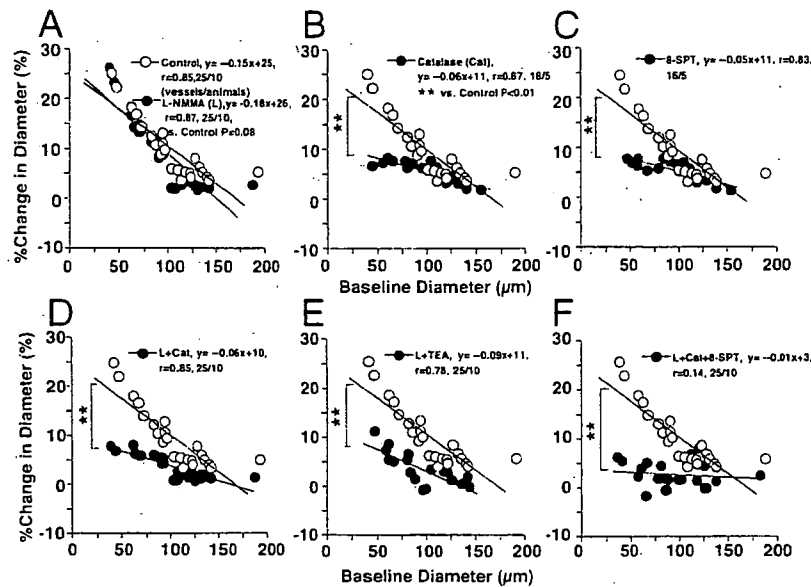


**Figure 2** Coronary Vascular Responses to Cardiac Pacing

The coronary vasodilating responses of both-sized coronary arteries were significantly inhibited in all experimental conditions except L-NMMA alone. \*\* $p < 0.01$ . Abbreviations as in Figure 1.

H<sub>2</sub>O<sub>2</sub> into water and oxygen); 4) adenosine receptor blockade alone (8-sulfophenyltheophylline [8-SPT], 25  $\mu\text{g}/\text{kg}/\text{min}$  IC for 5 min); 5) catalase plus L-NMMA; 6) catalase plus tetraethylammonium (TEA) (10  $\mu\text{g}/\text{kg}/\text{min}$  IC for 10 min, an inhibitor of large conductance K<sub>Ca</sub> channels to inhibit EDHF-mediated responses) (23); and 7) catalase plus L-NMMA with 8-SPT (16). These inhibitors were given at 30 min before cardiac tachypacing (Fig. 1). The basal coronary diameter was defined as that before pacing. We continuously observed the diameter change in subepicardial small coronary arteries ( $\geq 100 \mu\text{m}$ ) and arterioles ( $< 100 \mu\text{m}$ ) with an intravital microscope before and at 2 min after pacing. Microspheres were administered at 3 min after the pacing was started (Fig. 1). In the combined infusion protocol (L-NMMA+catalase+8-SPT), L-NMMA infusion was first started, followed by catalase infusion, and then 8-SPT was added at 15 min after the initiation of L-NMMA infusion (Fig. 1). Then, fresh and unfixed heart tissues were cut into several blocks and immediately frozen in optimal cutting temperature compound after the pacing. The flow and MVO<sub>2</sub> were measured as full-thickness values.

**Drugs.** All drugs were obtained from Sigma Chemical Co. and were diluted in a physiological saline immediately before use.

**Statistical analysis.** Results are expressed as means  $\pm$  SEM. Differences in the vasodilation of subepicardial coronary microvessels before and after pacing (Fig. 2) were examined by a multiple regression analysis using a model, in which the change in coronary diameter was set as a dependent variable (y) and vascular size as an explanatory variable (x), while the statuses of control and other inhibi-

tors were set as dummy variables (D1, D2) in the following equation:  $y = a_0 + a_1x + a_2D_1 + a_3D_2$ , where  $a_0$  through  $a_3$  are partial regression coefficients (16). Significance tests were made as simultaneous tests for slope and intercept differences. Pairwise comparisons against control were made without adjustment for multiple comparisons. The vessel was the unit of analysis without correction for correlated observations. The power of this analysis is greater than that of using the animal as the unit of analysis, giving smaller p values. Vascular fluorescent responses (Figs. 3 and 4) were analyzed by one-way analysis of variance followed by Scheffe's post hoc test for multiple comparisons. The criterion for statistical significance was at  $p < 0.05$ .

## Results

**Hemodynamic status and blood gases during pacing.** Throughout the experiments, mean aortic pressure was constant and comparable (Table 1), and pO<sub>2</sub>, pCO<sub>2</sub>, and pH were maintained within the physiological ranges (pO<sub>2</sub>  $> 70$  mm Hg, pCO<sub>2</sub> 25 to 40 mm Hg, and pH 7.35 to 7.45). Baseline coronary diameter was comparable in the absence and presence of inhibitors under the 7 different experimental conditions (Table 1). Cardiac tachypacing increased coronary blood flow and MVO<sub>2</sub> from the baseline values (Table 2, both  $p < 0.01$ ). Combined infusion of L-NMMA+catalase+8-SPT significantly decreased coronary blood flow (CBF) and MVO<sub>2</sub> as compared with control, L-NMMA alone (both  $p < 0.01$ ), catalase alone (both  $p < 0.01$ ), 8-SPT alone (both  $p < 0.01$ ), L-NMMA+catalase (both  $p < 0.05$ ), L-NMMA+TEA (both  $p < 0.05$ ). Com-

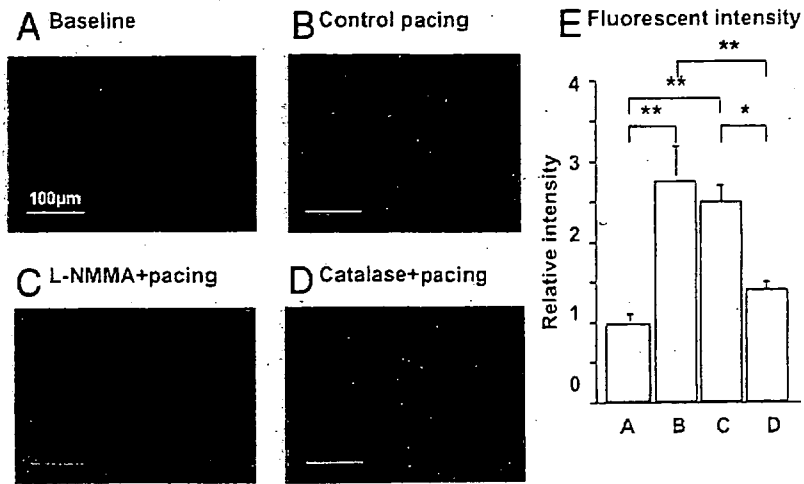


**Figure 3** Detection of H<sub>2</sub>O<sub>2</sub> Production With DCF Fluorescent Method

Hydrogen peroxide (H<sub>2</sub>O<sub>2</sub>) production was unaltered after N<sup>G</sup>-monomethyl-L-arginine (L-NMMA) but was markedly suppressed by catalase. Number of arterioles/animals used was 5/5 for each group. \*p < 0.05, \*\*p < 0.01. DCF = 2',7'-dichlorodihydrofluorescein diacetate.

bined infusion of L-NMMA+catalase or L-NMMA+TEA significantly decreased CBF (both p < 0.05) and MVO<sub>2</sub> (both p < 0.05) as compared with control after the pacing.

**Coronary vasodilation before and after cardiac tachypacing.** Cardiac tachypacing caused coronary vasodilation in both-sized arteries under control conditions (small coronary arteries, 5 ± 1%; arterioles, 14 ± 2%) (Fig. 2A) with decreased coronary venous pO<sub>2</sub> (Table 2). The metabolic coronary vasodilation was significantly decreased after L-NMMA in small coronary arteries (3 ± 1%) but not in arterioles (14 ± 2%), whereas catalase and 8-SPT decreased

the vasodilation of arterioles (both 4 ± 1%) but not in small coronary arteries (both 7 ± 1%) (Figs. 2B and 2C). Furthermore, the metabolic coronary vasodilation was markedly attenuated after L-NMMA+catalase and L-NMMA+TEA in small coronary arteries (both 2 ± 1%), and L-NMMA+catalase+8-SPT almost abolished the vasodilating responses in both-sized arteries (small coronary arteries, -1 ± 1%; arterioles, 1 ± 1%) (Figs. 2D to 2F). When expressed in a linear regression analysis, the coronary vasodilating responses of both-sized coronary arteries were significantly inhibited in all experimental conditions except L-NMMA alone (Fig. 2A).

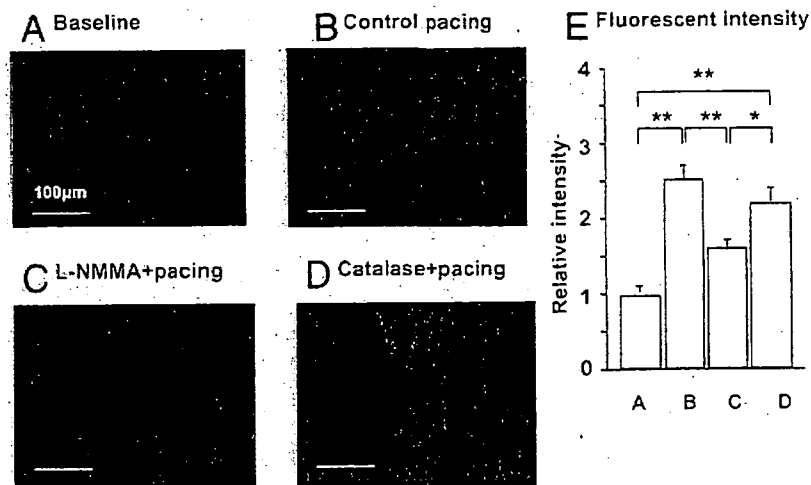


**Figure 4** Detection of NO Production With DAR Fluorescent Method

Nitric oxide (NO) production was unaltered after catalase but was markedly suppressed by N<sup>G</sup>-monomethyl-L-arginine (L-NMMA). Number of arterioles/animals used was 5/5 for each group. \*p < 0.05, \*\*p < 0.01. DAR = diamiorhodamine-4M AM.

**Table 1** The Small Artery and Arteriolar Diameter Measurements at Rest and During Cardiac Pacing

	Control	L-NMMA (L)	Catalase (Cat)	8-SPT	L+Cat	L+TEA	L+Cat+8-SPT
<b>Small artery</b>							
n (vessels/dogs)	12/10	12/10	9/5	7/5	12/10	12/10	12/10
Rest (μm)	127 ± 7	125 ± 6	127 ± 5	126 ± 6	125 ± 7	123 ± 6	124 ± 7
Cardiac pacing (μm)	134 ± 7*	129 ± 7†	132 ± 5*	131 ± 6*	127 ± 7	124 ± 6	123 ± 6
<b>Arteriole</b>							
n (vessels/dogs)	12/10	12/10	9/5	9/5	12/10	12/10	12/10
Rest (μm)	75 ± 5	73 ± 5	71 ± 5	71 ± 5	72 ± 5	74 ± 5	72 ± 6
Cardiac pacing (μm)	85 ± 5*	82 ± 5*	77 ± 6†	77 ± 6†	77 ± 5†	77 ± 5	73 ± 5

Results are expressed as mean ± SEM. \*p < 0.01, †p < 0.05 versus rest.  
L-NMMA = N<sup>G</sup>-monomethyl-L-arginine; SPT = sulfophenyltheophylline; TEA = tetraethylammonium.

**Detection of H<sub>2</sub>O<sub>2</sub> and NO production.** Fluorescent microscopy with DCF showed that cardiac tachypacing increased coronary H<sub>2</sub>O<sub>2</sub> production compared with baseline conditions in arterioles (Fig. 3). The pacing-induced H<sub>2</sub>O<sub>2</sub> production as assessed by DCF fluorescent intensity was unaltered after L-NMMA but was markedly suppressed by catalase (Fig. 3). By contrast, in small coronary arteries, vascular NO production as assessed by DAR fluorescent intensity was significantly increased in response to the pacing compared with baseline conditions (Fig. 4). The pacing-induced NO production was unaltered after catalase but was markedly suppressed by L-NMMA (Fig. 4). Pacing caused no significant increase in H<sub>2</sub>O<sub>2</sub> production in small coronary arteries or NO production in arterioles (data not shown).

**Discussion**

The major finding of the present study is that endogenous H<sub>2</sub>O<sub>2</sub> plays an important role in pacing-induced metabolic

coronary dilation as a compensatory mechanism for NO in vivo. We demonstrated the important role of endogenous H<sub>2</sub>O<sub>2</sub> in the mechanisms for metabolic coronary dilation in vivo. **Validations of experimental model and methodology.** We chose, on the basis of our previous reports (16,17), the adequate dose of L-NMMA, catalase, TEA, and 8-SPT in order to inhibit NO synthesis, H<sub>2</sub>O<sub>2</sub>, K<sub>Ca</sub> channels, and the adenosine receptor, respectively. The TEA at low doses is fairly specific for K<sub>Ca</sub> channel, but at higher doses it might block a number of other K channels. Because several K<sub>Ca</sub> channels might be involved in H<sub>2</sub>O<sub>2</sub>-mediated responses (5), we selected nonselective K<sub>Ca</sub> inhibitor, TEA, to inhibit all K<sub>Ca</sub> channels (23). We have previously confirmed the validity of our present methods (21).

**Role of NO and H<sub>2</sub>O<sub>2</sub> after cardiac pacing.** Matoba et al. have demonstrated that endothelium-derived H<sub>2</sub>O<sub>2</sub> is an EDHF in mouse (11) and human (12) mesenteric arteries and pig coronary microvessels (24). Morikawa et al. also

**Table 2** Hemodynamic Status at Rest and During Cardiac Pacing

	Control	L-NMMA (L)	Catalase (Cat)	8-SPT	L+Cat	L+TEA	L+Cat+8-SPT
n (dogs)	10	10	5	5	10	10	10
<b>SBP</b>							
Rest (mm Hg)	135 ± 14	135 ± 14	114 ± 9	123 ± 5	98 ± 9	99 ± 9	96 ± 8
Cardiac pacing	137 ± 14	136 ± 14	125 ± 12	130 ± 7	100 ± 9	100 ± 8	103 ± 9
<b>MBP</b>							
Rest (mm Hg)	117 ± 10	117 ± 10	98 ± 8	99 ± 5	89 ± 10	90 ± 10	87 ± 9
Cardiac pacing	124 ± 9	120 ± 13	107 ± 10	110 ± 7	91 ± 10	92 ± 10	92 ± 10
<b>DP</b>							
Rest	8,100 ± 845	8,100 ± 845	6,855 ± 527	7,350 ± 312	5,880 ± 537	5,910 ± 527	5,730 ± 478
Cardiac pacing	16,440 ± 1,718*	16,320 ± 1,680*	15,000 ± 1,423*	15,630 ± 778*	11,940 ± 11,029*	12,000 ± 1,011*	12,300 ± 1,078*
<b>CVPO<sub>2</sub></b>							
Rest (mm Hg)	20 ± 1	17 ± 1	16 ± 1	17 ± 1	15 ± 1†	15 ± 1†	14 ± 1†
Cardiac pacing	14 ± 1*	11 ± 1*	11 ± 1*	12 ± 1*	10 ± 1*†	10 ± 1*†	9 ± 1*†
<b>MVO<sub>2</sub></b>							
Rest (μlO <sub>2</sub> /min/g)	70 ± 2	66 ± 2	67 ± 2	73 ± 5	62 ± 5	61 ± 5	60 ± 5
Cardiac pacing	171 ± 4‡	168 ± 2‡	158 ± 12‡	168 ± 13‡	133 ± 4‡†	130 ± 18‡†	95 ± 9*§
<b>CBF</b>							
Rest (ml/min/g)	0.66 ± 0.06	0.63 ± 0.06	0.66 ± 0.03	0.66 ± 0.01	0.59 ± 0.06	0.62 ± 0.05	0.51 ± 0.04
Cardiac pacing	1.48 ± 0.32‡	1.46 ± 0.06‡	1.36 ± 0.02‡	1.40 ± 0.01‡	1.22 ± 0.01‡†	1.24 ± 0.12‡†	0.96 ± 0.07‡§

Results are expressed as mean ± SEM. \*p < 0.05 versus at rest. †p < 0.05 versus corresponding control measurements. ‡p < 0.01 versus rest. §p < 0.01 versus corresponding control measurements. CBF = coronary blood flow; CVPO<sub>2</sub> = coronary venous pO<sub>2</sub>; DP = double product; MBP = mean blood pressure; MVO<sub>2</sub> = myocardial oxygen consumption; SBP = systolic blood pressure; other abbreviations as in Table 2.

have demonstrated that endothelial Cu,Zn-SOD plays an important role as an H<sub>2</sub>O<sub>2</sub>/EDHF synthase in mouse (13) and human (14) mesenteric arteries. Subsequently, we (16,17) and others (15) confirmed that endogenous H<sub>2</sub>O<sub>2</sub> exerts important vasodilator effects in canine coronary microcirculation in vivo and in isolated human coronary microvessels, respectively. In the present study, the pacing-induced metabolic coronary vasodilation was significantly decreased after L-NMMA in small coronary arteries but not in arterioles, whereas catalase decreased the vasodilation of arterioles but not that of small arteries, and the coronary vasodilation was markedly attenuated after L-NMMA+catalase (Fig. 2). These findings indicate that NO and H<sub>2</sub>O<sub>2</sub> compensate for each other to maintain coronary vasodilation in response to increased myocardial oxygen demand. Coronary venous pO<sub>2</sub> tended to be lower after L-NMMA+catalase, suggesting that NO and H<sub>2</sub>O<sub>2</sub> coordinately cause coronary vasodilation during cardiac tachypacing.

Saitoh et al. (25) suggested that the production of H<sub>2</sub>O<sub>2</sub>, which stems from the dismutation of ·O<sub>2</sub><sup>-</sup> that is formed during mitochondrial electron transport, is seminal in the coupling between oxygen metabolism and blood flow in the heart. Thus, the contribution of H<sub>2</sub>O<sub>2</sub> production in response to the change in metabolism cannot be excluded.

Endothelial Cu,Zn-SOD plays an important role in the synthesis of H<sub>2</sub>O<sub>2</sub> as an EDHF synthase in mouse (13) and human (14) mesenteric arteries, and exercise training enhances expression of Cu,Zn-SOD in normal pigs (26). It remains to be examined whether exercise-induced up-regulation of Cu,Zn-SOD enhances metabolic coronary vasodilation mediated by endogenous H<sub>2</sub>O<sub>2</sub>.

**Compensatory vasodilator mechanism among H<sub>2</sub>O<sub>2</sub>, NO, and adenosine.** The EDHF acts as a partial compensatory mechanism to maintain endothelium-dependent vasodilation in the forearm microcirculation of patients with essential hypertension, where NO activity is impaired owing to oxidative stress (27). We have recently demonstrated in the fluorescent microscopy study that coronary vascular production of H<sub>2</sub>O<sub>2</sub> and NO is enhanced after myocardial ischemia/reperfusion in small coronary arteries and arterioles, respectively (17). In the present study, the DCF fluorescent intensity was comparable between control and L-NMMA, and that of DAR was also comparable between control and catalase (Figs. 3 and 4). Although the exact source of vascular production of H<sub>2</sub>O<sub>2</sub> and NO remains to be elucidated, it is highly possible that endothelium-derived NO and H<sub>2</sub>O<sub>2</sub> compensate for each other to maintain coronary vasodilation in response to increased MVO<sub>2</sub>.

In the dog, blockade of any vasodilator mechanisms fails to blunt the increase in coronary blood flow in response to exercise, indicating that adenosine, K<sup>+</sup><sub>ATP</sub>-channel opening, prostanooids, or NO might not be mandatory for exercise-induced coronary vasodilation, or that these redundant vasodilator mechanisms compensate for each other when one mechanism is blocked (28). In the present study,

adenosine blockade with 8-SPT alone inhibited the pacing-induced vasodilation of arteriole but not that of small artery, whereas combined administration of L-NMMA+catalase+8-SPT almost abolished the pacing-induced coronary vasodilation of both-sized arteries with an increase in coronary blood flow (Fig. 2). The discrepancy between the diameter and flow responses is likely due to the metabolic autoregulation of smaller arterioles. These results indicate that adenosine also plays an important role to maintain metabolic coronary vasodilation in cooperation with NO and H<sub>2</sub>O<sub>2</sub>, a finding consistent with our previous study on coronary autoregulatory mechanisms (15).

**Study limitations.** Several limitations should be mentioned for the present study. First, although we were able to demonstrate the production of H<sub>2</sub>O<sub>2</sub> with fluorescent microscopy with DCF, we were unable to quantify the endothelial H<sub>2</sub>O<sub>2</sub> production, because DCF reacts with H<sub>2</sub>O<sub>2</sub>, peroxyntirite, and hypochlorous acid (13). Second, we were unable to find smaller arterioles, owing to the limited spatial resolution of our charge-coupled device intravital microscope. With an intravital camera with higher resolution, we would be able to observe coronary vasodilation of smaller arterioles. Third, we were unable to determine whether H<sub>2</sub>O<sub>2</sub> is produced by shear stress or cardiac metabolism. This point remains to be elucidated in a future study.

## Conclusions

We were able to demonstrate that endogenous H<sub>2</sub>O<sub>2</sub> plays an important role in pacing-induced metabolic coronary vasodilation in canine coronary microcirculation in vivo and that there are substantial compensatory interactions among NO, H<sub>2</sub>O<sub>2</sub>, and adenosine to maintain metabolic coronary vasodilation, which is one of the most important mechanisms for cardiovascular homeostasis in vivo.

---

**Reprint requests and correspondence:** Dr. Toyotaka Yada, Department of Medical Engineering and Systems Cardiology, Kawasaki Medical School, 577 Matsushima, Kurashiki, Okayama 701-0192, Japan. E-mail: yada@me.kawasaki-m.ac.jp.

---

## REFERENCES

1. Ishibashi Y, Duncker DJ, Zhang J, Bache RJ. ATP-sensitive K<sup>+</sup> channels, adenosine, and nitric oxide-mediated mechanisms account for coronary vasodilation during exercise. *Circ Res* 1998;82:346-59.
2. Jones CJ, Kuo L, Davis MJ, DeFily DV, Chilian WM. Role of nitric oxide in the coronary microvascular responses to adenosine and increased metabolic demand. *Circulation* 1995;91:1807-13.
3. Yada T, Richmond KN, Van Bibber R, Kroil K, Feigl EO. Role of adenosine in local metabolic coronary vasodilation. *Am J Physiol* 1999;276:H1425-33.
4. Feletou M, Vanhoutte PM. Endothelium-dependent hyperpolarization of canine smooth muscle. *Br J Pharmacol* 1988;93:515-24.
5. Shimokawa H. Primary endothelial dysfunction: atherosclerosis. *J Mol Cell Cardiol* 1999;31:23-37.
6. Kuo L, Davis MJ, Chilian WM. Endothelium-dependent, flow-induced dilation of isolated coronary arterioles. *Am J Physiol* 1991; 259:H1063-70.

7. Kuo L, Chilian WM, Davis MJ. Interaction of pressure- and flow-induced responses in porcine coronary resistance vessels. *Am J Physiol* 1991;261:H1706-15.
8. Koller A, Sun D, Kaley G. Role of shear stress and endothelial prostaglandins in flow- and viscosity-induced dilation of arterioles in vitro. *Circ Res* 1993;72:1276-84.
9. Koller A, Sun D, Huang A, Kaley G. Corelease of nitric oxide and prostaglandins mediates flow-dependent dilation of rat gracilis muscle arterioles. *Am J Physiol* 1994;267:H326-32.
10. Takamura Y, Shimokawa H, Zhao H, et al. Important role of endothelium-derived hyperpolarizing factor in shear stress-induced endothelium-dependent relaxations in the rat mesenteric artery. *J Cardiovasc Pharmacol* 1999;34:381-7.
11. Matoba T, Shimokawa H, Nakashima M, et al. Hydrogen peroxide is an endothelium-derived hyperpolarizing factor in mice. *J Clin Invest* 2000;106:1521-30.
12. Matoba T, Shimokawa H, Kubota H, et al. Hydrogen peroxide is an endothelium-derived hyperpolarizing factor in human mesenteric arteries. *Biochem Biophys Res Comm* 2002;290:909-13.
13. Morikawa K, Shimokawa H, Matoba T, et al. Pivotal role of Cu,Zn-superoxide dismutase in endothelium-dependent hyperpolarization. *J Clin Invest* 2003;112:1871-9.
14. Morikawa K, Fujiki T, Matoba T, et al. Important role of superoxide dismutase in EDHF-mediated responses of human mesenteric arteries. *J Cardiovasc Pharmacol* 2004;44:552-6.
15. Miura H, Bosnjak JJ, Ning G, Saito T, Miura M, Gutterman DD. Role for hydrogen peroxide in flow-induced dilation of human coronary arterioles. *Circ Res* 2003;92:e31-40.
16. Yada T, Shimokawa H, Hiramatsu O, et al. Hydrogen peroxide, an endogenous endothelium-derived hyperpolarizing factor, plays an important role in coronary autoregulation in vivo. *Circulation* 2003;107:1040-5.
17. Yada T, Shimokawa H, Hiramatsu O, et al. Cardioprotective role of endogenous hydrogen peroxide during ischemia-reperfusion injury in canine coronary microcirculation in vivo. *Am J Physiol* 2006;291:H1138-46.
18. Jones CJ, DeFily DV, Patterson JL, Chilian WM. Endothelium-dependent relaxation competes with alpha 1- and alpha 2-adrenergic constriction in the canine epicardial coronary microcirculation. *Circulation* 1993;87:1264-74.
19. Scornik FS, Codina J, Birnbaumer L, Toro L. Modulation of coronary smooth muscle K<sub>Ca</sub> channels by Gs alpha independent of phosphorylation by protein kinase A. *Am J Physiol* 1993;265:H1460-5.
20. Tan CM, Xenoyannis S, Feldman RD. Oxidant stress enhances adenylyl cyclase activation. *Circ Res* 1995;77:710-7.
21. Yada T, Hiramatsu O, Kimura A, et al. In vivo observation of subendocardial microvessels of the beating porcine heart using a needle-probe videomicroscope with a CCD camera. *Circ Res* 1993;72:939-46.
22. Mori H, Haruyama Y, Shinozaki H, et al. New nonradioactive microspheres and more sensitive X-ray fluorescence to measure regional blood flow. *Am J Physiol* 1992;263:H1946-57.
23. Masumoto A, Hirooka Y, Shimokawa H, Hironaga K, Setoguchi S, Takeshita A. Possible involvement of Rho-kinase in the pathogenesis of hypertension in humans. *Hypertension* 2001;38:1307-10.
24. Matoba T, Shimokawa H, Morikawa K, et al. Electron spin resonance detection of hydrogen peroxide as an endothelium-derived hyperpolarizing factor in porcine coronary microvessels. *Arterioscler Thromb Vasc Biol* 2003;23:1224-30.
25. Saitoh S, Zhang C, Tune JD, et al. Hydrogen peroxide: a feed-forward dilator that couples myocardial metabolism to coronary blood flow. *Arterioscler Thromb Vasc Biol* 2006;26:2614-21.
26. Rush JW, Laughlin MH, Woodman CR, Price EM. SOD-1 expression in pig coronary arterioles is increased by exercise training. *Am J Physiol* 2000;279:H2068-76.
27. Taddei S, Versari D, Cipriano A, et al. Identification of a cytochrome P450 2C9-derived endothelium-derived hyperpolarizing factor in essential hypertensive patients. *J Am Coll Cardiol* 2006;48:508-15.
28. Duncker DJ, Bache RJ. Regulation of coronary vasomotor tone under normal conditions and during acute myocardial hypoperfusion. *Pharmacol Ther* 2000;86:87-110.



## Characterization of ouabain-induced noradrenaline and acetylcholine release from *in situ* cardiac autonomic nerve endings

T. Yamazaki,<sup>1</sup> T. Akiyama,<sup>1</sup> H. Kitagawa,<sup>1</sup> F. Komaki,<sup>1</sup> H. Mori,<sup>1</sup> T. Kawada,<sup>2</sup> K. Sunagawa<sup>2</sup> and M. Sugimachi<sup>2</sup>

<sup>1</sup> Department of Cardiac Physiology, National Cardiovascular Center Research Institute, Suita, Osaka, Japan

<sup>2</sup> Department of Cardiovascular Dynamics, National Cardiovascular Center Research Institute, Suita, Osaka, Japan

Received 11 January 2007,  
revision requested 28 March 2007,  
revision received 29 May 2007,  
accepted 30 June 2007  
Correspondence: T. Yamazaki,  
Department of Cardiac  
Physiology, National  
Cardiovascular Center Research  
Institute, 5-7-1 Fujishirodai, Suita,  
Osaka 565, Japan. E-mail:  
yamazaki@ri.ncvc.go.jp

### Abstract

**Aim:** Although ouabain modulates autonomic nerve ending function, it is uncertain whether ouabain-induced releasing mechanism differs between *in vivo* sympathetic and parasympathetic nerve endings. Using cardiac dialysis, we examined how ouabain induces neurotransmitter release from autonomic nerve ending.

**Methods:** Dialysis probe was implanted in left ventricle, and dialysate noradrenaline (NA) or acetylcholine (ACh) levels in the anaesthetized cats were measured as indices of neurotransmitter release from post-ganglionic autonomic nerve endings.

**Results:** Locally applied ouabain (100  $\mu\text{M}$ ) increased in dialysate NA or ACh levels. The ouabain-induced increases in NA levels remained unaffected by cardiac sympathetic denervation and tetrodotoxin ( $\text{Na}^+$  channel blocker, TTX), but the ouabain-induced increases in ACh levels were attenuated by TTX. The ouabain-induced increases in NA levels were suppressed by pretreatment with desipramine (NA transport blocker) and augmented by reserpine (vesicle NA transport blocker). In contrast, the ouabain-induced increases in ACh levels remained unaffected by pretreatment with hemicholinium-3 (choline transport blocker) but suppressed by vesamicol (vesicle ACh transport blocker). The ouabain-induced increases in NA levels were suppressed by pretreatment with  $\omega$ -conotoxin GVIA (N-type  $\text{Ca}^{2+}$  channel blocker), verapamil (L-type  $\text{Ca}^{2+}$  channel blocker) and TMB-8 (intracellular  $\text{Ca}^{2+}$  antagonist). The ouabain-induced increases in ACh levels were suppressed by pretreatment with  $\omega$ -conotoxin MVIIC (P/Q-type  $\text{Ca}^{2+}$  channel blocker), and TMB-8.

**Conclusions:** Ouabain-induced NA release is attributable to the mechanisms of regional exocytosis and/or carrier-mediated outward transport of NA, from stored NA vesicle and/or axoplasm, respectively, while the ouabain-induced ACh release is attributable to the mechanism of exocytosis, which is triggered by regional depolarization. At both sympathetic and parasympathetic nerve endings, the regional exocytosis is because of opening of calcium channels and intracellular calcium mobilization.

**Keywords** acetylcholine,  $\text{Ca}^{2+}$  channels, cat, microdialysis,  $\text{Na}^+$ ,  $\text{K}^+$ -AT-Pase, noradrenaline.

It is generally accepted that ouabain modulates autonomic nerve function by inhibition of membrane  $\text{Na}^+, \text{K}^+$ -ATPase (Gillis & Quest 1979). This neuronal modulatory effect was mainly reported with *in vitro* sympathetic (Sweadner 1985), parasympathetic nerve endings (Satoh & Nakazato 1992, Gomez *et al.* 1996) and adrenal glands (Haass *et al.* 1997). Furthermore, ouabain-induced modulatory effect was reported with *in vitro* studies on motor endplate (Vyskocil & Illes 1977, Zemkova *et al.* 1990). From these *in vitro* studies, several mechanisms are presently suggested to induce release of neurotransmitter from the nerve endings. However, it is uncertain whether the manner of modulation differs between *in vivo* sympathetic and parasympathetic nerve endings. A major concern is whether ouabain induces a brisk increase in neurotransmitter efflux (spontaneous neurotransmitter release). Kranzhöfer *et al.* (1991) reported that ouabain-induced spontaneous noradrenaline (NA) release from sympathetic nerve endings. On the other hand, ouabain-induced spontaneous acetylcholine (ACh) release was reported *in vitro* studies using synaptosomes (Satoh & Nakazato 1992). No reports have described *in vivo* spontaneous ACh release evoked by ouabain. Further, a second issue is at which site ouabain induces neurotransmitter release: stored vesicle or axoplasm (Haass *et al.* 1997). NA and ACh release have been reported in stored vesicles and/or the axoplasm. It is uncertain, however, which site induces the predominant neurotransmitter release evoked by ouabain *in vivo*. Furthermore, the mechanisms underlying the neurotransmitter release evoked by ouabain remain unclear. Neuronal effects of ouabain have been attributed to the inhibitory action upon  $\text{Na}^+, \text{K}^+$ -ATPase and transmembrane sodium pump (Haass *et al.* 1997). As a consequence of the reduced sodium gradient at the plasma membrane, two possible mechanisms have been proposed to induce NA release from nerve endings; (i) carrier-mediated reversed NA transport, and (ii)  $\text{Ca}^{2+}$ -dependent exocytotic NA release. The manner and mechanisms of NA efflux have been extensively studied and accepted *in vivo* in isolated tissues (Sweadner 1985, Haass *et al.* 1997). However, it remains unclear whether these assumptions are valid in the cardiac sympathetic or parasympathetic nerve endings *in vivo*.

Cardiac dialysis technique in combination with highly sensitive measurement of NA or ACh has offered a powerful method for detecting the low level of dialysate NA or ACh obtained from the myocardial space (Akiyama *et al.* 1991, 1994). We demonstrated that dialysate NA or ACh levels were affected by local administration of pharmacological agents through dialysis probes, indicating that changes in dialysate NA or ACh levels reflect NA or ACh output from cardiac postganglionic sympathetic or parasympathetic nerve end-

ings (Yamazaki *et al.* 1997, Kawada *et al.* 2001) respectively. Using dialysis technique, ouabain can be administered locally and it is possible to monitor NA or ACh output following locally applied ouabain (Yamazaki *et al.* 2001). Furthermore, comparison of the dialysate NA response in the presence and absence of neuronal agents can differentiate carrier-mediated NA release from calcium dependent exocytotic NA release (Yamazaki *et al.* 1997). With locally applied neuronal blockers, we examined the mechanisms and the sites underlying NA or ACh release evoked by ouabain.

## Methods

### Animal preparation

Adult cats were anaesthetized with pentobarbital sodium (30–35 mg  $\text{kg}^{-1}$  i.p.). The level of anaesthesia was maintained with a continuous intravenous infusion of pentobarbital sodium (1–2 mg  $\text{kg}^{-1}$   $\text{h}^{-1}$ ). The animals were intubated and ventilated with room air mixed with oxygen. Body temperature was maintained using a heated pad and lamp. All protocols were performed in accordance with the National Cardiovascular Center Research Institute Animal Care Ethics Committee guidelines that were in strict compliance with the NIH Guide for the Care and Use of Laboratory Animals. Electrocardiogram and mean arterial pressure were simultaneously monitored with a data recorder. The sixth rib on the left side was resected to expose the heart. With a fine guiding needle, one or two dialysis probes for dialysate sampling were implanted in the mid wall of the anterolateral region of the left ventricle. Heparin (100 U  $\text{kg}^{-1}$ ) was administered after implantation of the dialysis probe and a maintenance dose was given every hour thereafter.

### Dialysis technique

The material and properties of the dialysis probe were described previously (Akiyama *et al.* 1991, 1994). Briefly, we designed a transverse dialysis probe. Both ends of a dialysis fibre (13 mm length, 0.31 mm o.d. and 0.2 mm i.d.; PAN-1200, 50 000 molecular weight cutoff, Asahi Chemical, Tokyo, Japan) were connected and glued to polyethylene tubes (25 cm length, 0.5 mm o.d. and 0.2 mm i.d.). The dialysate NA or ACh levels were measured in separate animals. For the measurement of dialysate NA, the dialysis probe was perfused with Ringer's solution at 10  $\mu\text{L min}^{-1}$ . Sampling periods were 2 min in duration (one sample volume = 20  $\mu\text{L}$ ), which was the minimum period necessary to collect sufficient NA for satisfactory measurement. For the measurement of dialysate ACh, Ringer's solution containing eserine (choline esterase

inhibitor, 100  $\mu\text{M}$ ) was perfused at 2  $\mu\text{L min}^{-1}$  and sampling periods were 15 min in duration. Dialysate sampling was started 120 min after probe implantation, when the dialysate NA or ACh concentration had reached a steady level. Each sample was collected in a microtube containing 0.1 N HCl or phosphate buffer to prevent oxidation. The dead-space volume between the dialysis and sample tube was measured. Taking this dead-space into account, samples were obtained.

### Experimental protocols

In our previous study, we demonstrated that the dialysate NA or ACh levels reflect cardiac neuronal NA or ACh disposition at the nerve endings (Yamazaki *et al.* 1997, Kawada *et al.* 2001). Therefore, in the present study, we obtained dialysate samples and measured the dialysate NA or ACh levels as an index of NA or ACh output from post-ganglionic sympathetic or parasympathetic nerve endings respectively. Generally two mechanisms and sites are proposed to induce NA and ACh release from nerve endings: exocytotic (quantum) release from the stored vesicle and non-exocytotic (non-quantum) release from the axoplasm. The present studies were designed to clarify whether ouabain-induced NA or ACh efflux are affected by local administration of pharmacological agents that modify experimental conditions.

*Protocol 1: Time courses of dialysate NA and ACh levels during local administration of ouabain.* We examined the time course of dialysate NA and ACh levels during local administration of ouabain (100  $\mu\text{M}$ ). Ouabain was administered for 60 min. Dialysate NA levels were measured before and at 10-min intervals during ouabain administration. Dialysate ACh levels were collected in consecutive 15-min sampling periods.

*Protocol 2: Influence of nerve transection and  $\text{Na}^+$  channels on dialysate NA or ACh response evoked by ouabain.* To test whether ouabain modulated central-mediated exocytotic neurotransmitter release, we examined the time course of ouabain-induced dialysate NA and ACh levels after transection of stellate ganglia or cervical parasympathetic nerve tract. For cardiac sympathetic denervation, the region of the stellate ganglia was exposed through the intercostal space, and bilateral transection of stellate ganglia was performed. After cardiac sympathetic denervation, heart rate response to carotid occlusion was blunted. In separate cats, cervical vagotomy was performed. We started dialysate sampling at 120 min after surgical interruption and ouabain-induced NA or ACh efflux was examined. Furthermore, to examine involvement of depolarization on NA or ACh release, ouabain-induced NA or ACh

efflux was measured with addition of tetrodotoxin (TTX, 10  $\mu\text{M}$ ) through the dialysis probe. At 60 min after the beginning of TTX administration, we started the control sampling and examined the ouabain-induced NA or ACh response.

*Protocol 3: Influence of NA-, ACh- and choline transporters on dialysate NA or ACh response evoked by ouabain.* To test whether ouabain-induced neurotransmitter efflux was derived from axoplasm or stored vesicle, ouabain-induced NA or ACh efflux was examined with local administration of pharmacological agents, which affected the transport and content of neurotransmitter at the nerve endings. Membrane carrier-mediated NA transport was blocked by local administration of desipramine, whereas vesicular NA import was blocked by local administration of reserpine. In either case, ouabain-induced NA efflux was examined with the addition of desipramine (100  $\mu\text{M}$ ) or reserpine (10  $\mu\text{M}$ ) through the dialysis probe. The dosage of agent-administration was decided after referring to the previous studies (Akiyama *et al.* 1994, Yamazaki *et al.* 1997). Membrane carrier-mediated choline transport was blocked by local administration of hemicholinium-3 (10  $\mu\text{M}$ ), whereas vesicular ACh import was blocked by local administration of vesamicol (10  $\mu\text{M}$ ) (Kawada *et al.* 2001). In either case, ouabain-induced ACh efflux was examined with the addition of hemicholinium-3 or vesamicol through the dialysis probe.

*Protocol 4: Influence of  $\text{Ca}^{2+}$  transporter, channel, mobilization on dialysate NA or ACh response evoked by ouabain.* To test the contention that ouabain-induced neurotransmitter efflux was modulated by changes in intracellular  $\text{Ca}^{2+}$  levels, the influence of  $\text{Ca}^{2+}$  transporter, channel, mobilization on the dialysate NA or ACh response evoked by ouabain was examined. We focused on the involvement of three types of voltage-dependent  $\text{Ca}^{2+}$  channel, the L- and N types in the NA release evoked by ouabain. Sixty minutes after starting local administration of verapamil (100  $\mu\text{M}$ ), or  $\omega$ -conotoxin GVIA (10  $\mu\text{M}$ ), we measured the ouabain-induced NA response. Second, we examined the involvement of plasma membrane  $\text{Na}^+/\text{Ca}^{2+}$  exchanger in the NA release evoked by ouabain. The inhibitors of membrane  $\text{Na}^+/\text{Ca}^{2+}$  exchange (dechlorobezamil; 100  $\mu\text{M}$ , or KB7943; 10  $\mu\text{M}$ ) were locally administered through the dialysis probe and the ouabain-induced NA response was measured. Third, we examined the involvement of intracellular  $\text{Ca}^{2+}$  level in the NA release evoked by ouabain. An intracellular  $\text{Ca}^{2+}$  antagonist [3,4,5-trimethoxybenzoic acid 8-(diethyl amino)-octyl ester (TMB-8)] blocks the efflux of calcium from intracellular calcium stores without affecting influx

(Wiedenkeller & Sharp 1984). TMB-8 (1 mM) was locally administered through the dialysis probe and ouabain-induced NA response was measured. A similar pharmacological intervention was performed and ouabain-induced ACh responses were measured. Sixty minutes after starting local administration of verapamil (100  $\mu\text{M}$ ), or  $\omega$ -conotoxin GVIA (10  $\mu\text{M}$ ),  $\omega$ -conotoxin MVIIC (10  $\mu\text{M}$ ), we measured the ouabain-induced ACh response. The inhibitor of membrane  $\text{Na}^+/\text{Ca}^{2+}$  exchange (KB7943; 10  $\mu\text{M}$ ) was locally administered through the dialysis probe and the ouabain-induced ACh response was measured. Third, an intracellular  $\text{Ca}^{2+}$  antagonist (TMB-8, 1 mM) was locally administered through the dialysis probe and ouabain-induced ACh response was measured.

#### Analytical procedure

Dialysate NA concentrations were measured by HPLC with electrochemical detection (HPLC-ECD; Eicom, Kyoto, Japan). An alumina procedure was performed to remove the interfering compounds from the dialysate. The detection limit was 50 fmol per injection. Dialysate ACh concentration was measured directly by another HPLC-ECD. The detection limit was 50 fmol per injection. Details of HPLC-ECD for the NA and ACh measurements have been described elsewhere (Akiyama *et al.* 1991, 1994).

At the end of each experiment, the cats were killed with an overdose of pentobarbital sodium, and the implant sites were checked to confirm that the dialysis probes had been implanted within the left ventricular myocardium. Statistical analysis of the data was performed by analysis of variance (ANOVA). Statistical significance was defined as  $P < 0.05$ . Values are presented as mean  $\pm$  SE.

## Results

#### Protocol 1: Time course of dialysate NA and ACh levels during local administration of ouabain

Although local administration of ouabain did not affect haemodynamic parameters including heart rate, mean arterial pressure and electrocardiogram, ouabain induced the efflux of NA. Figure 1 (upper panel) shows the time course of the dialysate NA levels during local administration of ouabain (100  $\mu\text{M}$ ). Dialysate NA level increased significantly from  $0.18 \pm 0.06 \text{ nmol L}^{-1}$  at control to  $2.39 \pm 0.53 \text{ nmol L}^{-1}$  at 10,  $12.92 \pm 1.39 \text{ nmol L}^{-1}$  at 20 min and  $14.79 \pm 1.97 \text{ nmol L}^{-1}$  at 30 min. Subsequently, a slow decline occurred but high dialysate NA levels were maintained during locally applied ouabain. Peak level of dialysate NA ranged from 20 to 30 min after the beginning of ouabain adminis-

tration. Figure 1 (lower panel) shows the time course of the dialysate ACh levels during local administration of ouabain (100  $\mu\text{M}$ ). Dialysate ACh level increased significantly from  $0.91 \pm 0.05 \text{ nmol L}^{-1}$  at control to  $3.6 \pm 0.60 \text{ nmol L}^{-1}$  at 0–15,  $8.1 \pm 1.4 \text{ nmol L}^{-1}$  at 15–30 min and  $6.8 \pm 1.25 \text{ nmol L}^{-1}$  at 30–45 min. Peak level of dialysate ACh appeared at 15–30 min after the beginning of ouabain administration.

#### Protocol 2: Influence of denervation and TTX on dialysate NA and ACh responses evoked by ouabain

We sampled the dialysates over 60 min of ouabain administration. To compare ouabain-induced NA or ACh levels under various interventions, ouabain-induced dialysate NA or ACh levels were subtracted from the control values. The sum of relative changes in dialysate NA or ACh (the unit:  $\Sigma\text{nmol/L}$ ) was expressed as an index of total NA or ACh release evoked by ouabain. Figure 2 (upper panel) shows the total NA release evoked by ouabain when cardiac sympathetic nerves were either intact, transected, pretreated with TTX. The ouabain-induced total NA release did not differ among them. Figure 2 (lower panel) shows the total ACh release evoked by ouabain when cardiac parasympathetic nerves were either intact, transected, or pretreated with TTX. The ouabain-induced total ACh release did not differ between the intact cardiac parasympathetic nerve and denervated groups whereas addition of TTX significantly inhibited the total ACh release by approx. 57% of vehicle.

#### Protocol 3: Influence of transport blocking agents on dialysate NA and ACh responses evoked by ouabain

Figure 3 (upper panel) shows the total NA release evoked by ouabain among various pharmacological interventions. Pretreatment with reserpine caused significant augmentation of the ouabain-induced total NA release whereas pretreatment with desipramine caused significant suppression of the total NA release. Figure 3 (lower panel) shows the total ACh release evoked by ouabain among various pharmacological interventions. The ouabain-induced total ACh release did not differ between the intact and hemicholinium-3 pretreated groups whereas addition of vesamicol significantly inhibited the total ACh release by approx. 45% of vehicle.

#### Protocol 4: Influence of $\text{Ca}^{2+}$ mobilization on dialysate NA and ACh responses evoked by ouabain

Figure 4 (upper panel) shows the total NA release evoked by ouabain among various  $\text{Ca}^{2+}$  interventions. The total NA release in the 60 min after administration